ADVANCES IN ATMOSPHERIC SCIENCES, VOL. 31, NOVEMBER 2014, 1245–1255

The Response of the East Asian Summer Monsoon to Strong Tropical Volcanic Eruptions

CUI Xuedong[1,2], GAO Yongqi*[1,3,4], and SUN Jianqi[1]

[1]*Nansen-Zhu International Research Centre, Institute of Atmospheric Physics, Chinese Academy of Sciences, Beijing* 100029

[2]*University of Chinese Academy of Sciences, Beijing* 100049

[3]*Nansen Environmental and Remote Sensing Center, Bergen, Norway*

[4]*Bjerknes Center for Climate Research, University of Bergen, Bergen, Norway*

(Received 28 November 2013; revised 24 April 2014; accepted 29 April 2014)

ABSTRACT

A 600-year integration performed with the Bergen Climate Model and National Centers for Environmental Prediction/National Center for Atmospheric Research (NCEP/NCAR) reanalysis data were used to investigate the impact of strong tropical volcanic eruptions on the East Asian summer monsoon (EASM) and EASM rainfall. Both the simulation and NCEP/NCAR reanalysis data show a weakening of the EASM in strong eruption years. The model simulation suggests that North and South China experience droughts and the Yangtze–Huaihe River Valley experiences floods during eruption years. In response to strong tropical volcanic eruptions, the meridional air temperature gradient in the upper troposphere is enhanced, which leads to a southward shift and an increase of the East Asian subtropical westerly jet stream (EASWJ). At the same time, the land–sea thermal contrast between the Asian land mass and Northwest Pacific Ocean is weakened. The southward shift and increase of the EASWJ and reduction of the land–sea thermal contrast all contribute to a weakening of the EASM and EASM rainfall anomaly.

Key words: East Asian summer monsoon, volcanic eruption, East Asian subtropical westerly jet stream, land–sea thermal contrast

Citation: Cui, X. D., Y. Q. Gao, and J. Q. Sun, 2014: The response of the East Asian summer monsoon to strong tropical volcanic eruptions. *Adv. Atmos. Sci.*, **31**(6), 1245–1255, doi: 10.1007/s00376-014-3239-8.

1. Introduction

Volcanic eruptions are an important external forcing for climate change on seasonal to multidecadal timescales (Robock, 2000; Shindell et al., 2004; Emile-Geay et al., 2008). Strong volcanic eruptions, by increasing aerosol loading in the stratosphere, generally cool the surface through negative radiative forcing (e.g., Angell and Korshover, 1985; Robock, 2000; D'Arrigo et al., 2008). Previous studies have shown that strong volcanic eruptions have impacts on summer precipitation at the global scale (e.g., Mass and Portman, 1989; Yoshimori et al., 2005; Schneider et al., 2009; Cui et al., 2014). However, early studies have also suggested that the impact of volcanic eruptions on precipitation is not as obvious as that on temperature (e.g., Gillett et al., 2004; Lambert et al., 2005; Fischer et al., 2007).

The East Asian summer monsoon (EASM) is an important societal influence for East Asian countries including China, Japan and Korea. In fact, the EASM brings 40%–50% of annual rainfall to the Yangtze–Huaihe River region, and 60%–70% to North China (Gong and Ho, 2003). In recent decades, EASM rainfall in eastern China has increased in its southern domain (Yangtze–Huaihe River Valley) and decreased in its northern domain (Xu, 2001; Gong and Ho, 2002; Wu et al., 2006). Although the cause of this precipitation pattern is still under debate, early studies have suggested that it could be attributed, or at least partly attributed, to the climate effects of aerosols (Xu, 2001; Menon et al., 2002; Wang et al., 2013). Observation- and reconstruction-based studies, as well as numerical simulations, have indicated that volcanic eruptions might have an effect on the EASM and summer rainfall over eastern China. For example, by analyzing data from meteorological stations, Xu (1986) described wet conditions in the Yangtze–Huaihe River Valley region, and drought conditions in North China, after three strong volcanic eruptions. Liu et al. (1993), by analyzing reconstructed drought/flood index in China for the past 500 years, found substantial differences in the spatial and temporal evolution of the drought/flood pattern in response to volcanic eruptions

* Corresponding author: GAO Yongqi
E-mail: gyq@mail.iap.ac.cn

at low and mid-high latitudes. They showed that there are more frequent drought events in North and South China in response to low-latitude volcanic eruptions, whereas significant positive rainfall anomalies can occur over the Yangtze–Huaihe River Valley region in the following years. Jiang et al. (2005) showed that frequent strong fluctuations of wet and drought conditions occurred in the Yangtze–Huaihe River Valley after the eruption of Tambora in 1815. Some studies have suggested strong low-latitude volcanic eruptions could cause coherent drought over the whole of eastern China, but that mid–high-latitude volcanic eruptions have no significant effect on precipitation over the region in the eruption year, and the following year, based on reconstructed drought/flood data (Shen et al., 2008; Schneider et al., 2009; Zhang et al., 2013). Peng et al. (2009) and Zhang et al. (2013), using climate model simulations, also found a reduction in summer rainfall over the whole of eastern China in response to strong volcanic eruptions, and suggested this rainfall anomaly may be caused by a weakening of the EASM. However, there are studies that have analyzed the last 500 years of large volcanic activities and corresponding drought/flood conditions in summer in China, and these have suggested a wide range in the positive rainfall anomaly response over eastern China (Zhang and Zhang, 1985; Zhang and Zhang, 1994). In brief, the response of summer rainfall over eastern China to strong volcanic eruptions is not yet clear.

Possible mechanisms through which volcanic eruptions impact upon the EASM and EASM rainfall have been proposed. Liu et al. (1993) suggested volcanic eruptions increase the SST in the equatorial eastern Pacific (Handler, 1986; Handler and Andsager, 1990). The SST in the equatorial eastern Pacific plays an important role in regulating drought/wet conditions in eastern China (e.g., Chang et al., 2000; Yu et al., 2009). Shen et al. (2007) suggested volcanic eruptions could cause increased winter snow cover over the Eurasian continent and the following cool summers, leading to a weakened EASM through a reduction of the land–sea thermal contrast. Besides, lower temperatures in summer may enhance the high ridge or blocking situation over East Siberia, making the subtropical high shift farther south and cause droughts over North China and wetter conditions in the Yangtze–Huaihe River Valley. Peng et al. (2009) indicated volcanic eruptions decrease the thermal contrast between the Asian land mass and surrounding oceans, meanwhile leading to a weakened water vapor source for eastern China due to a decline in evaporation over the tropical oceans. However, these early proposed mechanisms focus mainly on the response of lower-tropospheric circulation to volcanic eruptions. Due to massive amounts of dust and gases being injected into the stratosphere after volcanic eruptions, climate anomalies in the stratosphere and upper troposphere may play an important role in modulating the EASM and EASM rainfall.

In this study, we examine the response of the EASM and summer (June–August, JJA) rainfall over eastern China to strong volcanic eruptions by using observed data and a 600-year integration of the Bergen Climate Model (BCM; Otterå et al., 2009), and explore changes in both high- and low-level atmospheric circulation.

2. Model simulation and methods

The BCM is a fully coupled atmosphere–ocean–sea ice climate model. The atmospheric component is the spectral general circulation model, Action de Recherche Petite Echelle Grande Echelle (ARPEGE; Déqué et al., 1994). In this study, ARPEGE is run at T63 horizontal resolution ($\sim 2.8^\circ$ in latitude and longitude), and a time step of 1800 seconds. A total of 31 vertical levels are employed, ranging from the surface to 0.01 hPa (20 levels in the troposphere). The oceanic component is the Miami Isopycnic Coordinate Ocean Model (MICOM), with a total of 34 vertical layers (Bleck et al., 1992). With the exception of the equatorial region, the ocean model has an almost regular horizontal grid spacing of approximately $2.4^\circ \times 2.4^\circ$. The horizontal spacing in the meridional direction is gradually decreased to 0.8° along the equator to better resolve the dynamics near the equator. The sea ice model is Global Experimental Leads and sea ice model for ATmosphere and Ocean (GELATO), which is described in detail in Salas-Melia (2002). The Ocean Atmosphere Sea Ice Soil (OASIS, version 2) coupler is used to couple the various model components. The model can run stably for many centuries without any form of flux adjustments. For more details, please refer to Cui et al. (2013).

The multiple century simulation used is a 600-year integration (Otterå et al., 2009), which includes external forcings due to the variation in total solar irradiance (TSI) and the changes in the amount of stratospheric aerosols following explosive volcanic eruptions for the last 600 years (1400–1999). The other forcings are kept constant. The TSI forcing field is from Crowley et al. (2003), and is based on a reconstruction (Lean et al., 1995) after 1610. The forcing field is provided as variations in the effective solar constant. This will in turn modify the top of the atmosphere shortwave flux. The volcanic aerosol forcing time series (Crowley et al., 2003) are supplied as monthly optical depths at 0.55 μm in the middle of the visible spectrum, and applied to the model in the form of monthly quarter-spherical means in four bands (30°–90°N, 0°–30°N, 0°–30°S, 30°–90°S). Beginning in the 1960s, modern observations are used instead of reconstructed data. The aerosol loading is distributed through each model level in the stratosphere using a weighting function (Otterå, 2008). The volcanic mass of the stratospheric aerosols are then calculated at each grid point and model level in the stratosphere by dividing the total aerosol concentration by the total air mass of all stratospheric levels at that grid point. Only the direct effect of stratospheric aerosol has been taken into account. The original aerosol loading values have been converted to radiative forcing according to Sato et al. (1993). The variations in TSI and radiative forcing from volcanic eruptions are shown in Fig. 1.

In this study, 18 strong volcanic events during the last 600 years are chosen with an anomalous negative radiative forc-

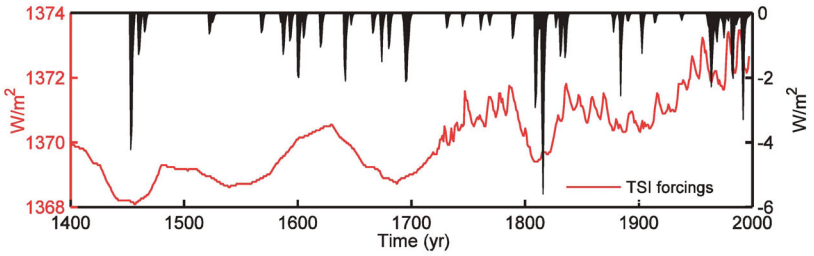

Fig. 1. Time series of the total solar irradiance forcing (red) and the radiative forcing from volcanic eruptions (black).

Table 1. Strong tropical volcanic eruption years based on Crowley et al. (2003) and the first summer times after eruptions for the SEA and composite analysis. VEI is the Volcanic Explosivity Index.

Eruption description					
Year	Name	Latitude	Radiative forcing	VEI	First summer after the eruptions (June–July–August, JJA)
1453	Kuwae	16.8°S	−4.2	6	JJA (1453)
1460	Unknown		−1.3		JJA (1460)
1586	Kelut	7.9°S	−1.3	5	JJA (1587)
1600	Huaynaputina	16.6°S	−1.9	6	JJA (1600)
1620	Unknown		−1.1		JJA (1620)
1641	Parker	6.1°N	−1.7	5	JJA (1642)
1674	Gamnokara	1.4°N	−1.5	5	JJA (1674)
1680	Unknown		−1.1		JJA (1680)
1693	Serusa	6.3°S	−1.1	4	JJA (1694)
1809	Unknown		−2.9		JJA (1809)
1815	Tambora	8.3°S	−5.6	7	JJA (1816)
1831	Babuyan Claro	19.5°N	−1.3	4	JJA (1831)
1835	Cosiguina	13.0°N	−1.4	5	JJA (1835)
1883	Krakatau	6.1°S	−2.6	6	JJA (1884)
1902	Santa Maria	14.8°N	−1.3	6	JJA (1903)
1963	Agung	8.3°S	−1.9	4	JJA (1964)
1982	El Chicon	17.4°N	−2.1	5	JJA (1982)
1991	Pinatubo	15.1°N	−3.3	6	JJA (1992)

ing larger than 1 W m^{-2} (Table 1). In addition to the model data, the National Centers for Environmental Prediction/National Center for Atmospheric Research (NCEP/NCAR) reanalysis data (Kalnay et al., 1996) and monthly rainfall from the Climate Research Unit (CRU) (New et al., 1999) are used to examine the influence of strong volcanic eruptions on the EASM and EASM rainfall over eastern China. A superposed epoch analysis (SEA; Haurwitz and Brier, 1981), which is a statistical method used to resolve significant signal-to-noise ratios is employed. The mean values of climate variables from summer in year −8 to summer in year 8, with year 0 being the first summer after an eruption, are used as the reference climatology. The bootstrap method (Efron and Tibshirani, 1986) is used to test the statistical significance of the SEA. We reshuffle with replacement the elements from the available time span to generate a new random sample and average the sample into a new epoch composite. Then, the above process is repeated 10 000 times and confidence intervals are evaluated by the 95% and 99% spread of the composite results.

3. Results

3.1. *Performance of the BCM's representation of the EASM*

Summer rainfall, low-level winds and the 200 hPa jet stream are generally used to describe variations in the EASM (e.g., Wang, 2001; Zhang et al., 2006). The BCM has been evaluated to be capable of reproducing the distribution and intensity of observed summer precipitation (Cui et al., 2013). Figure 2 shows the climatological JJA mean fields of 850 hPa and 200 hPa horizontal winds in the NCEP/NCAR reanalysis and model. The model captures the main feature of lower-tropospheric circulation (spatial correlation coefficient of 0.86 for the area shown in the figure). For example, the model successfully reproduces the spatial patterns of cross-equatorial flow over South Asia and anticyclonic cir-

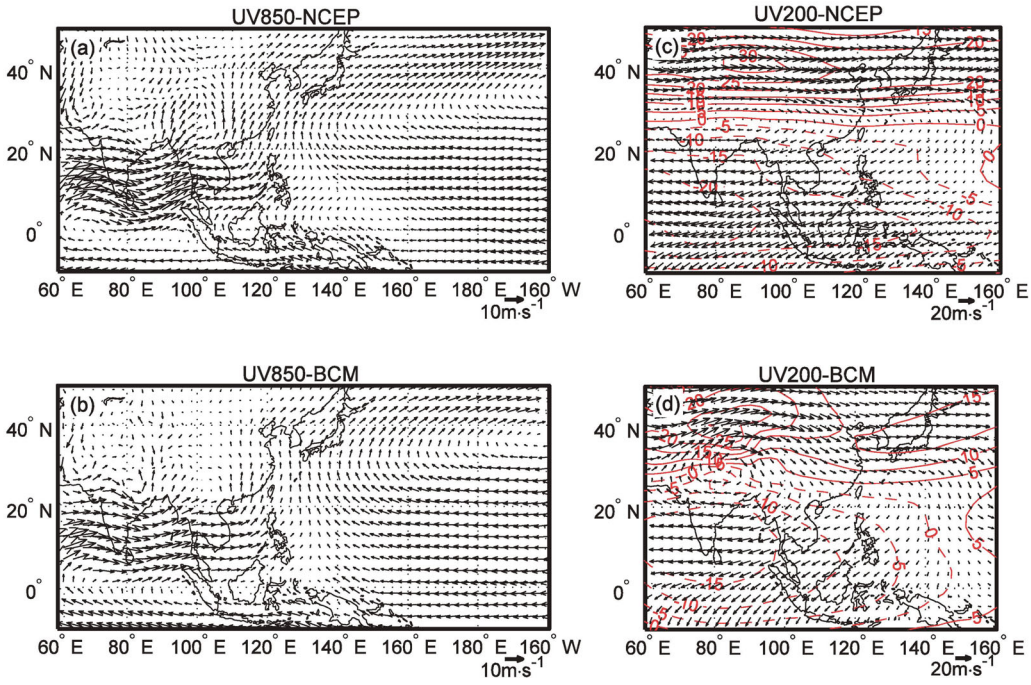

Fig. 2. Spatial distributions of JJA mean (a, b) 850 hPa and (c, d) 200 hPa horizontal wind vectors. Panels (a) and (c) are based on NCEP/NCAR reanalysis data, while panels (b) and (d) are from the BCM. Red contours indicate the mean zonal wind at 200 hPa. Units: m s^{-1}.

culation over the western Pacific subtropical high (WPSH) region. The model also reproduces the location and characteristics of the summer East Asian subtropical westerly jet stream (EASWJ). The EASWJs in the NCEP/NCAR reanalysis and model are both located at approximately 35°–45°N and have maximum centers over the Eurasian continent and eastern Asia. However, the simulated EASWJ is weaker and inclines towards the northeast.

3.2. *The effects of volcanic eruptions in the BCM*

We use the EASM index defined by Wang (2000) as the area-mean (20°–40°N, 110°–125°E) velocity at 850 hPa (represented by its anomaly to the climatology). When the EASM is stronger, the stronger low-level flow carries more water vapor toward the north, inducing a positive summer rainfall anomaly over North China and a negative one over the Yangtze–Huaihe Valley. Figure 3a shows the change in EASM index before and after 18 strong volcanic eruption cases during the last 600 years. During strong volcanic eruption years, the occurrence probability of a weak summer monsoon is significantly higher than the mean at the 95% confidence level, showing a significant subsequent anomalous northerly over eastern China (Fig. 3b). The summer rainfall response during the first summer after eruptions is illustrated in Fig. 4. It shows negative rainfall anomalies over North and South China, whereas positive anomalies are found over the Yangtze–Huaihe Valley and south of Japan, which is consistent with the results from instrumental and reconstructed data (Xu, 1986; Liu et al., 1993). This spatial pattern of anomalous rainfall is similar to the "wet in the south–

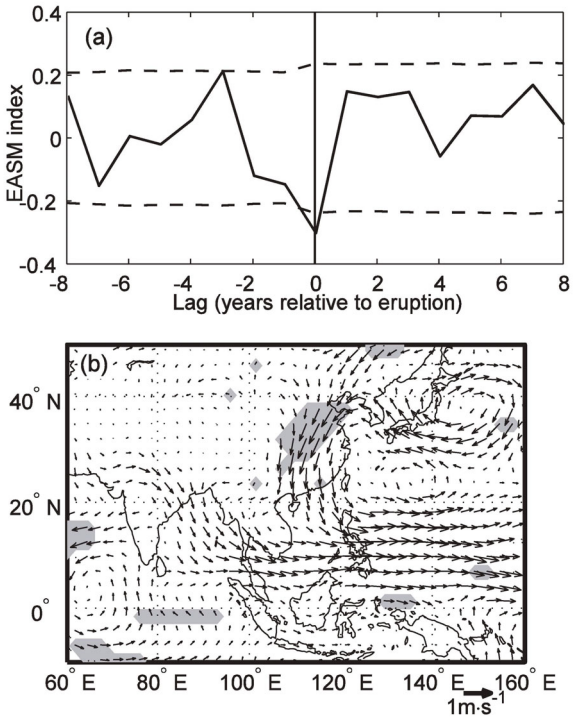

Fig. 3. (a) Superposed epoch analysis for the simulated EASM index. Dashed lines indicate the 95% confidence level. Units: m s^{-1}. (b) Composite anomaly of simulated summer horizontal wind at 850 hPa during the first summer after eruptions; areas with anomalies significant at the 95% confidence level are shaded. Units: m s^{-1}.

drought in the north" pattern seen over eastern China in recent decades, indicating the rainfall anomaly in our model is associated with a weakening of the EASM. Due to the reduction in southerly winds in eastern China during the weakened EASM period, less moisture is carried from the ocean to eastern China, and enhanced moisture convergence takes place over the Yangtze–Huaihe Valley (Fig. 5).

In order to understand the mechanisms underlying the response of the EASM and EASM rainfall to strong volcanic eruptions, we examine the anomalies of associated oceanic and atmospheric variables during the first post-eruption summer for the 18 strong volcanic eruption cases during the last 600 years. Figure 6a shows the composite of summer zonally averaged air temperature anomalies. Because large amounts of volcanic aerosols are injected into the atmosphere in tropical regions, the largest increase in air temperature appears at the bottom of the low-latitude stratosphere, where anomalies reach up to 2 K. In addition, a significant cooling signal is found in the troposphere due to the scattering of incoming shortwave radiation. However, the tropospheric cooling is stronger in the high latitudes, producing an enhanced meridional temperature gradient. This may be caused by the positive feedback of sea ice (Robock, 1983; Robock, 2000) and has also been discussed by Wang et al. (2012). Figure 6b shows the composite of the summer mean temperature averaged in the upper troposphere between 200 hPa and 500 hPa. The region of significant cooling covers a large area in the mid- and high-latitudes (north of about 38°N), which contributes to a positive meridional air temperature gradient in the upper troposphere. Previous studies have noted that the upper-tropospheric meridional temperature gradient is responsible for the location and strength of the EASWJ (e.g., Wallace and Hobbs, 1977; Zhang et al., 2006; Zhang and Huang, 2011). According to the principle of thermal wind,

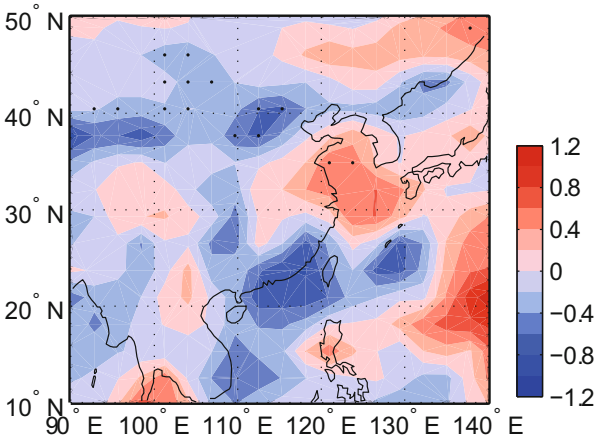

Fig. 4. Composite anomaly of simulated summer precipitation (units: mm d^{-1}) during the first summer after eruptions; areas marked by black dots indicate the 95% confidence level.

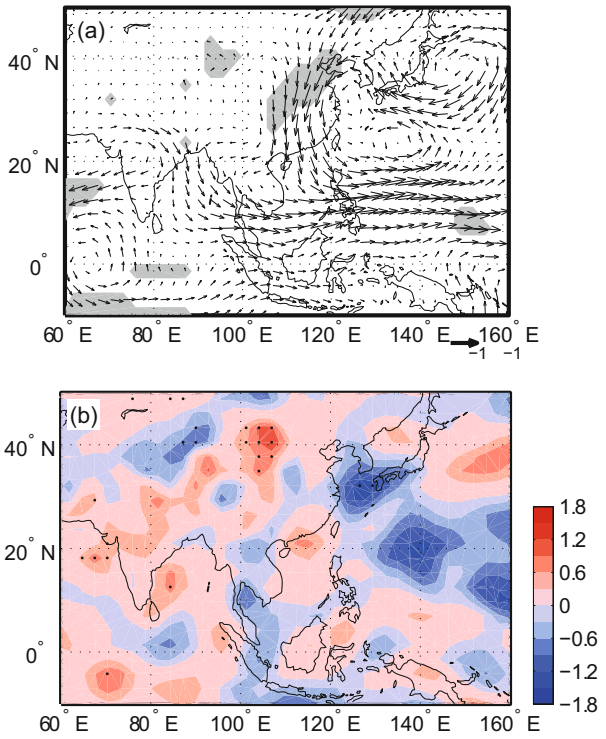

Fig. 5. Composite anomaly of (a) simulated summer vertical integrated moisture flux (units: 40 kg m^{-1} s^{-1}) and (b) its divergence (units: mm d^{-1}) during the first summer after eruptions. For moisture flux, areas with anomalies significant at the 95% confidence level are shaded. For divergence, areas marked by black dots indicate the 95% confidence level.

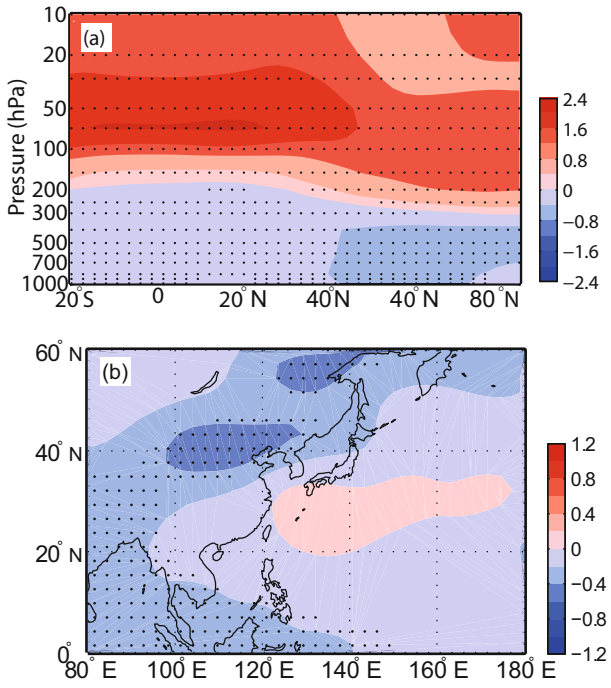

Fig. 6. Composite anomaly of simulated summer (a) zonal mean air temperature and (b) mean upper-tropospheric (500–200 hPa) air temperature during the first summer after eruptions. Areas marked by black dots indicate the 95% confidence level. Units: °C.

westerly anomalous winds are found over the mid-latitude regions of East Asia and the Northwest Pacific in the upper troposphere during the eruption years (Fig. 7a). The pattern of anomalous winds results in the EASWJ over East Asia shifting southward and gaining in strength. From the results of the SEA on the simulated EASWJ index, which is defined by the summer zonal wind at 200 hPa averaged over the region where the climatological zonal wind speed is greater than 15 m s^{-1}, we find that the EASWJ is significantly enhanced during the eruption years (Fig. 7b). Owing to the coupling of upper- and lower-tropospheric jet streams, these anomalies of the EASWJ produce a secondary circulation (Uccellini and Johnson, 1979; Lu et al., 2011). In the upper levels, anomalous cyclonic circulation is generated to the left side of the upper jet stream's core, and anomalous anticyclonic circulation to the right side of its core. The upper-tropospheric wind response during the volcanic eruption years reveals the presence of anticyclonic anomalies in the subtropical western North Pacific and cyclonic anomalies in northeastern China (Fig. 7a). In the lower levels, the south side of the upper jet stream's core generates convergence and ascending flow. In contrast, on the north side, divergence and descending flow are generated. Obvious anomalous cyclonic winds at lower levels are found in Fig. 5a. Due to the secondary circulation, the EASM circulation is therefore weakened and summer rainfall is suppressed along the Yangtze–Huaihe Valley. Previous other studies have also shown that the intensified and southward-shifted EASWJ induces a weakening of the EASM and leads to more precipitation occurring along the Yangtze–Huaihe Valley, and less over South and North China (e.g., Liang and Wang, 1998; Yu et al., 2004; Yang and Zhang, 2007).

The response of summer SST in the first post-eruption summer is weak. The model does not show any statistically significant negative SST anomaly in the Pacific Ocean (Fig. 8a). Instead, significant surface temperature cooling occurs over the Asian continent (Fig. 8b), leading to a decrease in the land–sea temperature gradient. It should be noted here that negative anomalies in SST are found in most Pacific regions in the following eruption years (figure not shown). The EASM is part of the Hadley circulation, which is related to both hemispheres. The EASM circulation is usually considered as a reversed Hadley cell since its direction is opposite to that of the northern Hadley cell (Riehl et al., 1950; Zhou and Li, 2002; Chen et al., 2010). The local Hadley circulation in the EASM region (105°–130°E) is described by regional meridional mass streamfunction and displayed in Fig. 9a. The JJA mean Hadley circulation is characterized by rising motion near the equator, upper-level poleward flow, sinking motion in the subtropics, and lower-level equatorward flow, resulting in an enclosed cell, which is similar to the observation (figure not shown). Due to the decrease in the land–sea thermal contrast between the tropical ocean and the Asian continent, significant positive mass streamfunction anomalies are present at 20°–40°N (Fig. 9b) during the first post-eruption summer, indicating a weakening of the reversed Hadley circulation. The anomalous Hadley circulation is

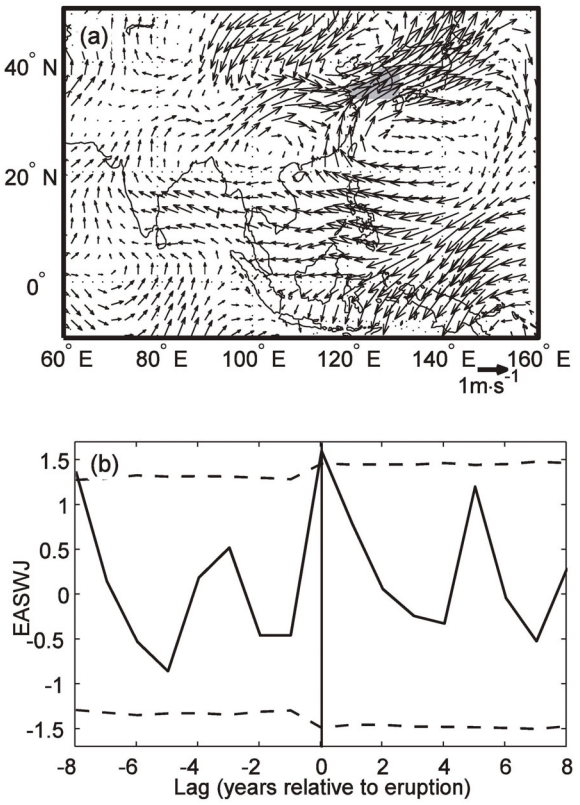

Fig. 7. (a) Composite anomaly of simulated summer horizontal wind at 200 hPa during the first summer after eruptions. Areas with anomalies significant at the 95% confidence level are shaded. Units: mm d^{-1}. (b) Superposed epoch analysis for the simulated EASWJ index. Dashed lines indicate the 95% confidence level. Units: m s^{-1}.

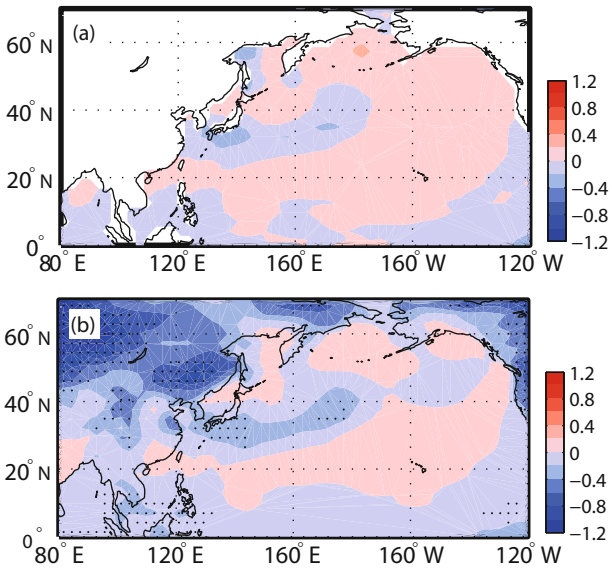

Fig. 8. Composite anomaly of simulated summer (a) sea surface temperature and (b) surface temperature during the first summer after eruptions. Areas marked by black dots indicate the 95% confidence level. Units: °C.

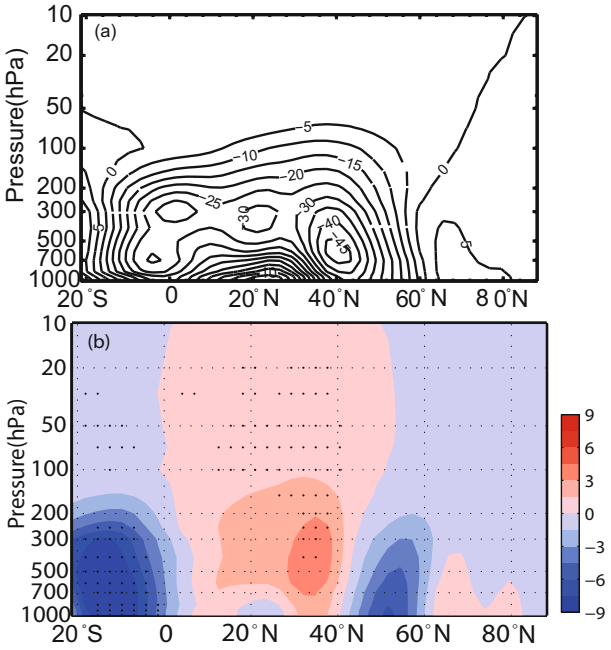

Fig. 9. (a) Mean state of the simulated regional meridional mass streamfunction (105°–140°E; units: 10^{10} kg s^{-1}) for JJA. (b) Cross sections of the composite meridional mass streamfuction anomalies during the first summer after eruptions. Areas marked by black dots indicate 95% confidence level.

associated with a weakened EASM (Sun and Zhou, 2014)

The above analysis illustrates that strong volcanic eruptions could lead to a weakened EASM and increased rainfall in the Yangtze–Huaihe Valley, whereas decreased rainfall in North and South China, in the first summer after eruptions. Our results indicate that strong volcanic eruptions can lead to an intensified and southward-shifted EASWJ by inducing a positive meridional air temperature gradient in the upper troposphere, and can also lead to reduced land–sea thermal contrast between the Asian continent and the surrounding oceans, mainly due to lowered air temperature over land. These changes all result in EASM rainfall anomalies and a weakening of the EASM.

3.3. *The effects of volcanic eruptions in the NCEP/NCAR reanalysis*

Similar effects of strong volcanic eruptions on the EASM can also be found in the NCEP/NCAR reanalysis during the past decades. There are four strong tropical volcanos that erupted after the year 1948: Agung (1963), Fuego (1974), EL Chichón (1982) and Pinatubo (1991). After these strong volcanic eruptions, a weakening trend is found in the EASM (Fig. 10a). From the results of the SEA on the detrended EASM index for these four cases during the last 60 years (Fig. 10b), a significant weakening is found in the EASM. Besides, anomalous southerly winds across eastern China after the strong volcanic eruptions are shown in Fig. 10c. Note that the weakened EASM happens in the same year if the volcanic eruption is before the summer, whereas is happens in the

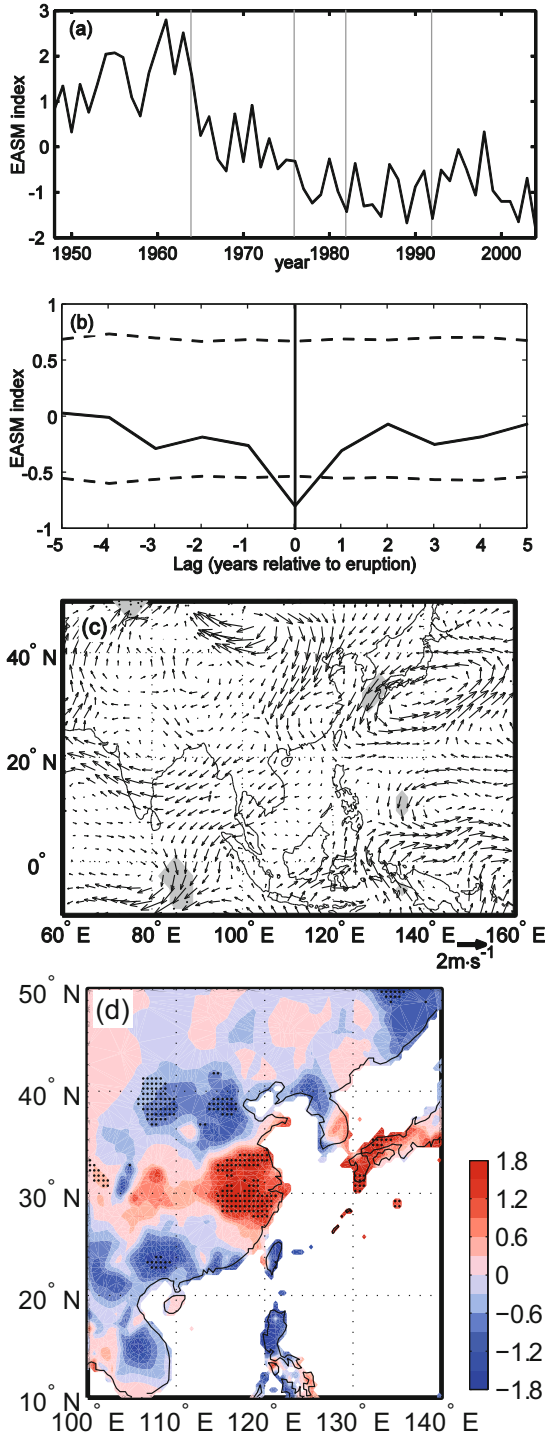

Fig. 10. (a) Temporal variation of East Asian summer monsoon index (units: m s^{-1}) from the NCEP/NCAR reanalysis. Vertical lines represent the strong volcanic eruptions in the tropics. (b) Superposed epoch analysis for the detrended EASM index. Dashed lines indicate the 95% confidence level. (c) Composite anomaly of horizontal wind (units: m s^{-1}) at 850 hPa during the volcanic eruption summer. (d) Composite anomaly of observed summer precipitation from the CRU (units: mm d^{-1}) during the volcanic eruption year. Areas shaded and marked by dots in Figs.10 c and d indicate the 95% confidence level.

following year if the volcanic eruption happens after summer. Meanwhile, increased summer rainfall in the Yangtze–Huaihe Valley, and decreased summer rainfall over North China is found in the CRU rainfall data (Fig. 10d). A similar pattern in rainfall anomalies was also reported by Xu (1986).

Similarly, stronger tropical heating in the lower stratosphere can also be found in the NCEP/NCAR reanalysis in the volcanic eruption years. In addition, the troposphere cools following volcanic eruptions, with the cooling being stronger at high latitudes (Fig. 11a). A strong decrease in summer temperature in the upper troposphere is evident at the mid and high latitudes north of about 32°N (Fig. 11b), which produces an enhanced equator-to-pole temperature gradient in the upper troposphere. As a result, the EASWJ over East Asia shifts southward and is intensified (Fig. 11c), which corresponds to a weakening of the EASM via the physical process described in section 3.2. However, there is no significant thermal contrast between the Asian land mass and surrounding oceans following the strong volcanic eruptions in the NCEP/NCAR reanalysis. Therefore, the effects of strong volcanic eruptions on the EASM in the NCEP/NCAR reanalysis are mainly manifested through the interactions between upper- and lower-tropospheric circulations. It should be mentioned that the response of the equator-to-pole temperature gradient and winds in the upper troposphere in the NCEP/NCAR is stronger than the results from the BCM.

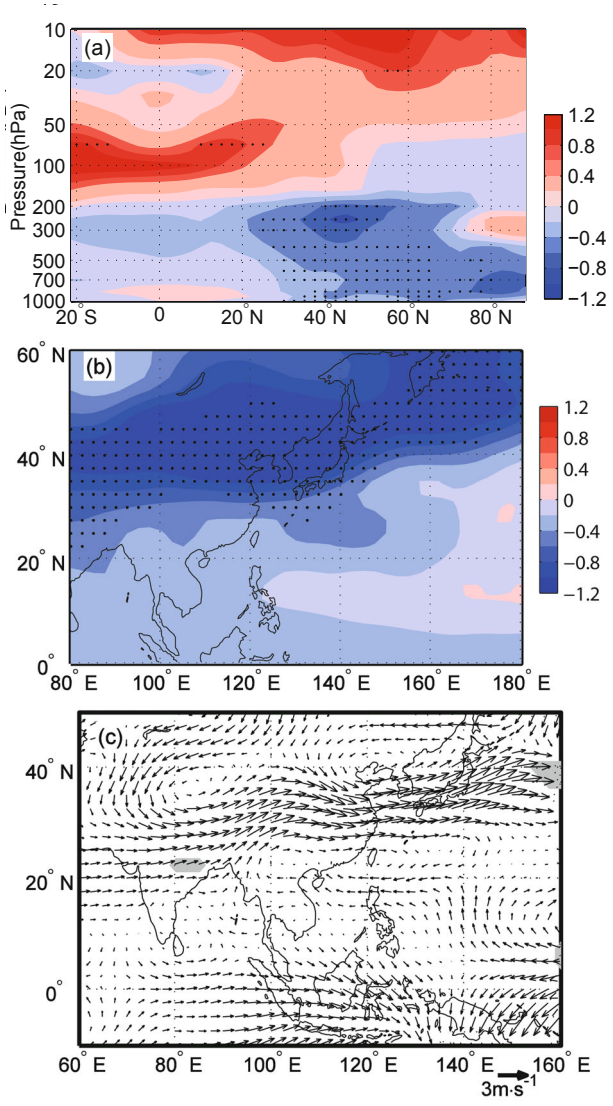

Fig. 11. Composite anomaly of (a) zonal mean air temperature, (b) mean upper-tropospheric (500–200 hPa) air temperature, and (c) horizontal wind at 200 hPa during the second post-eruption summer. Areas marked by black dots indicate the 95% confidence level.

4. Discussion and conclusion

Our analysis indicates that the EASM weakened after the four strong volcanic eruptions covered by NCEP/NCAR reanalysis data. Meanwhile, many studies have revealed that the EASM experienced a distinct weakening during the past 50 years, with a transition occurring from the mid-1960s to the end of the 1970s (Wang, 2000, 2001; Xue, 2001), and being characterized by a pronounced increase in rainfall over the Yangtze–Huaihe River Valley and a decrease in its flank (Gong and Ho, 2002; Zhang et al., 2004; Liu et al., 2011). Early studies suggested that the weakening of the EASM can be attributed to human-induced activities (Chang et al., 2009; Mahmood and Li, 2011; Wang and Fan, 2013). Besides, there is another transition of precipitation pattern between the 1980s–1990s in which the rainfall is reduced in central China and increased in northern, western, and southern China, which is more related to increased loading of anthropogenic aerosols, such as black carbon (Gu et al., 2010). There were two strong volcanos (Agung and Fuego in the years 1963 and 1975, respectively) that erupted during the period of this EASM weakening. It is difficult to draw a certain conclusion on the relationship between the EASM weakening and strong volcanic eruptions during the NCEP/NCAR period. The weakening of the EASM and the eruption of strong volcanos may be unrelated, or just a coincidence in time. What we have shown is that strong volcanic eruptions could lead to a weakening of the EASM in the eruption year. Furthermore, using the 600-yr BCM simulation to investigate the effect of strong volcanos on the EASM and EASM rainfall, we found that—similar to the results from the NCEP/NCAR reanalysis—volcanic eruptions led to a weakening of the EASM and associated EASM rainfall anomalies over the past 600 years. Therefore, our results are consistent with Liu et al. (1993), but differ from Shen et al. (2008), Schneider et al. (2009) and Zhang et al. (2013), who suggested drought over eastern China following strong volcanic eruptions.

Compared to previous studies (Peng et al., 2009), the time series of volcanic forcing used in our simulation provides information about monthly and latitudinal distributions of the volcanic aerosols. We focused on the climate response to strong high-latitude and low-latitude volcanic eruptions. However, a deficiency in terms of the spatial distribution of volcanic aerosol is imposed in only four latitude bands, and questions over the suitability of this representation of aerosol

have been raised before (Otterå, 2008; Marshall et al., 2009). The impact of volcanic eruptions on climate is the closest natural analogue to sulfate aerosol geoengineering, the implementation of which, in simple terms, targets a reduction of global solar irradiance. However, in reality, the climatic processes related to volcanic eruptions are much more complicated. For example, the chemical effects of enhanced stratospheric aerosol abundance from volcanic eruptions need to be considered (McKeen et al., 1984; Eyring et al., 2006).

In this research, we used a fully coupled climate model, the BCM, and NCEP/NCAR reanalysis data, to investigate the response of the EASM and EASM rainfall to strong tropical volcanic eruptions. Our results can be summarized as follows:

In the model, and in the NCEP/NCAR reanalysis, a weakening of the EASM can be found after strong tropical volcanic eruptions. Besides, increased rainfall in the Yangtze–Huaihe Valley and decreased rainfall in North and South China during eruption years can also be found in the model. The possible mechanism underlying the response of the EASM to strong volcanic eruptions was investigated and discussed. It is suggested that, firstly, strong volcanic eruptions induce a positive meridional air temperature gradient in the upper troposphere, which leads to a southward-shifted and intensified EASWJ. Secondly, strong volcanic eruptions weaken the land–sea thermal contrast between the Asian land mass and surrounding oceans. The changes in the EASWJ and the land–sea thermal contrast result in a weakening of the EASM and EASM rainfall anomalies.

Acknowledgements. This work was supported by the Strategic Priority Research Program (Grant No. XDA05110203) of the Chinese Academy of Sciences, the Research Council of Norway through the India-Clim project, and the National Basic Research Program of China (Grant Nos. 2012CB955401 and 2010CB951802). The authors are also grateful to Dr. Odd Helge OTTERÅ for the model output.

REFERENCES

Angell, J., and J. Korshover, 1985: Surface temperature changes following the six major volcanic episodes between 1780 and 1980. *J. Climate Appl. Meteor.*, **24**(9), 937–951.

Bleck, R., C. Rooth, D. Hu, and L. T. Smith, 1992: Salinity-driven thermocline transients in a wind-and thermohaline-forced isopycnic coordinate model of the North Atlantic. *J. Phys. Oceanogr.*, **22**, 1486–1486.

Chang, C. P., Y. S. Zhang, and T. Li, 2000: Interannual and interdecadal variations of the East Asian summer monsoon and tropical Pacific SSTs. Part I: Roles of the subtropical ridge. *J. Climate*, **13**(24), 4310–4325.

Chang, W. Y., H. Liao, and H. J. Wang, 2009: Climate responses to direct radiative forcing of anthropogenic aerosols, tropospheric ozone, and long-lived greenhouse gases in eastern China over 1951–2000. *Adv. Atmos. Sci.*, **26**(4), 748–762, doi: 10.1007/s00376-009-9032-4.

Chen, H. M., T. J. Zhou, R. B. Neale, X. Q. Wu, and G. J. Zhang, 2010: Performance of the new NCAR CAM 3.5 in East Asian summer monsoon simulations: Sensitivity to modifications of the convection scheme. *J. Climate*, **23**, 3657–3675.

Crowley, T. J., S. K. Baum, K. Y. Kim, G. C. Hegerl, and W. T. Hyde, 2003: Modeling ocean heat content changes during the last millennium. *Geophys. Res. Lett.*, **30**(18), 1932, doi: 10.1029/2003GL017801.

Cui, X. D., Y. Q. Gao, D. Y. Gong, D. Guo, and T. Furevik, 2013: Teleconnection between winter Arctic Oscillation and Southeast Asian summer monsoon in the pre-industry simulation of a coupled climate model. *Atmos. Oceanic Sci. Lett.*, **6**, 349–354.

Cui, X. D., Y. Q. Gao, J. Q. Sun, D. Guo, S. L. Li, and O. M. Johannessen, 2014: Role of natural external forcing factors in modulating the Indian summer monsoon rainfall, the winter North Atlantic Oscillation and their relationship on interdecadal timescale. *Climate Dyn.*, doi: 10.1007/s00382-014-2053-4.

D'Arrigo, R., R. Wilson, and A. Tudhope, 2008: The impact of volcanic forcing on tropical temperatures during the past four centuries. *Nature Geosci.*, **2**(1), 51–56.

Déqué, M., C. Dreveton, A. Braun, and D. Cariolle, 1994: The ARPEGE/IFS atmosphere model: A contribution to the French community climate modelling. *Climate Dyn.*, **10**(4), 249–266.

Efron, B., and R. Tibshirani, 1986: Bootstrap methods for standard errors, confidence intervals, and other measures of statistical accuracy. *Statistical Science*, **1**, 54–75.

Emile-Geay, J., R. Seager, M. A. Cane, E. R. Cook, and G. H. Haug, 2008: Volcanoes and ENSO over the past millennium. *J. Climate*, **21**(13), 3134–3148.

Eyring, V., and Coauthors, 2006: Assessment of temperature, trace species, and ozone in chemistry-climate model simulations of the recent past. *J. Geophy. Res.*, **111**, D22308, doi: 10.1029/2006JD007327.

Fischer, E. M., J. Luterbacher, E. Zorita, S. F. B. Tett, C. Casty, and H. Wanner, 2007: European climate response to tropical volcanic eruptions over the last half millennium. *Geophys. Res. Lett.*, **34**, L05707, doi: 10.1029/2006GL027992.

Gu, Y., K. Liou, W. Chen, and H. Liao, 2010: Direct climate effect of black carbon in China and its impact on dust storms. *J. Geophys. Res.*, **115**(D7), D00K14, doi: 10.1029/2009JD013427.

Gillett, N. P., A. J. Weaver, F. W. Zwiers, and M. F. Wehner, 2004: Detection of volcanic influence on global precipitation. *Geophys. Res. Lett.*, **31**(12), L12217, doi: 10.1029/2004GL020044.

Gong, D. Y., and C. H. Ho, 2002: Shift in the summer rainfall over the Yangtze River valley in the late 1970s. *Geophys. Res. Lett.*, **29**(10), 1436, doi: 10.1029/2001GL014523.

Gong, D. Y., and C. H. Ho, 2003: Arctic oscillation signals in the East Asian summer monsoon. *J. Geophys. Res.*, **108**(D2), 4066, doi: 10.1029/2002JD002193.

Handler, P., 1986: Possible association between the climatic effects of stratospheric aerosols and sea surface temperatures in the eastern tropical Pacific Ocean. *J. Climatol.*, **6**(1), 31–41.

Handler, P., and K. Andsager, 1990: Volcanic aerosols, El Niño and the Southern Oscillation. *Int. J. Climatol.*, **10**(4), 413–424.

Haurwitz, M. W., and G. W. Brier, 1981: A critique of the superposed epoch analysis method: Its application to solar-weather relations. *Mon. Wea. Rev.*, **109**(10), 2074–2079.

Jiang, T., Q. Zhang, R. Blender, and K. Fraedrich, 2005: Yangtze

Delta floods and droughts of the last millennium: Abrupt changes and long term memory. *Theor. Appl. Climatol.*, **82**, 131–141.

Kalnay, E., and Coauthors, 1996: The NCEP/NCAR 40-year reanalysis project. *Bull. Amer. Meteor. Soc.*, **77**(3), 437–471.

Lambert, F. H., N. P. Gillett, D. A. Stone, and C. Huntingford, 2005: Attribution studies of observed land precipitation changes with nine coupled models. *Geophys. Res. Lett.*, **32**(18), L18704, doi: 10.1029/2005GL023654.

Lean, J., J. Beer, and R. Bradley, 1995: Reconstruction of solar irradiance since 1610: Implications for climate change. *Geophys. Res. Lett.*, **22**(23), 3195–3198.

Liang, X. Z., and W. C. Wang, 1998: Associations between China monsoon rainfall and tropospheric jets. *Quart. J. Roy. Meteor. Soc.*, **124**(552), 2597–2623.

Liu, Y., G. Huang, and R. H. Huang, 2011: Inter-decadal variability of summer rainfall in Eastern China detected by the Lepage test. *Theor. Appl. Climatol.*, **106**(3-4), 481–488.

Liu, Y. Q., Y. H. Li, and P. Q. Jia, 1993: A comparative analysis of effect of volcanic eruptions at low and mid-high latitudes on drought/flood in China. *Meteorological Monthly*, **19**(11), 3–7. (in Chinese)

Lu, R., H. Ye, and J. G. Jhun, 2011: Weakening of interannual variability in the summer East Asian upper-tropospheric westerly jet since the mid-1990s. *Adv. Atmos. Sci.*, **28**(6), 1246–1258, doi: 10.1007/s00376-011-0222-5.

Mahmood, R., and S. L. Li, 2011: Modeled influence of East Asian black carbon on inter-decadal shifts in East China summer rainfall. *Atmos. Oceanic Sci. Lett.*, **4**(6), 349–355.

Marshall, A. G., A. A. Scaife, and S. Ineson, 2009: Enhanced seasonal prediction of European winter warming following volcanic eruptions. *J. Climate*, **22**(23), 6168–6180.

Mass, C. F., and D. A. Portman, 1989: Major volcanic eruptions and climate: A critical evaluation. *J. Climate*, **2**(6), 566–593.

McKeen, S. A., S. C. Liu, and C. S. Kiang, 1984: On the chemistry of stratospheric SO_2 from volcanic eruptions. *J. Geophys. Res.*, **89**(D3), 4873–4881.

Menon, S., J. Hansen, L. Nazarenko, and Y. Luo, 2002: Climate effects of black carbon aerosols in China and India. *Science*, **297**(5590), 2250–2253.

New, M., M. Hulme, and P. Jones, 1999: Representing twentieth-century space-time climate variability. Part I: Development of a 1961–90 mean monthly terrestrial climatology. *J. Climate*, **12**(3), 829–856.

Otterå, O. H., 2008: Simulating the effects of the 1991 Mount Pinatubo volcanic eruption using the ARPEGE atmosphere general circulation model. *Adv. Atmos. Sci.*, **25**(2), 213–226, doi: 10.1007/s00376-008-0213-3.

Otterå, O. H., M. Bentsen, I. Bethke, and N. G. Kvamst, 2009: Simulated pre-industrial climate in Bergen Climate Model (version 2): Model description and large-scale circulation features. *Geosci. Model Dev.*, **2**, 197–212.

Peng, Y. B., C. M. Shen, W.-C. Wang, and Y. Xu, 2009: Response of summer precipitation over Eastern China to large volcanic eruptions. *J. Climate*, **23**(3), 818–824.

Robock, A., 1983: Ice and snow feedbacks and the latitudinal and seasonal distribution of climate sensitivity. *J. Atmos. Sci.*, **40**(4), 986–997.

Robock, A., 2000: Volcanic eruptions and climate. *Rev. Geophys.*, **38**(2), 191–220.

Riehl, H., T. Yeh, and R. Sutcliffe, 1950: The intensity of the net meridional circulation. *Quart. J. Roy. Meteor. Soc.*, **76**(328), 182–188.

Salas-Melia, D., 2002: A global coupled sea ice-ocean model. *Ocean Modelling*, **4**(2), 137–172.

Sato, M., J. E. Hansen, M. P. McCormick, and J. B. Pollack, 1993: Stratospheric aerosol optical depths, 1850–1990. *J. Geophys. Res.*, **98**(D12), 22 987–22 994.

Schneider, D. P., C. M. Ammann, B. L. Otto-Bliesner, and D. S. Kaufman, 2009: Climate response to large, high-latitude and low-latitude volcanic eruptions in the Community Climate System Model. *J. Geophys. Res.*, **114**, D15101, doi: 10.1029/2008JD011222.

Shen, C. M., W. C. Wang, Z. X. Hao, and W. Gong, 2007: Exceptional drought events over eastern China during the last five centuries. *Climatic Change*, **85**, 453–471.

Shen, C. M., W. C. Wang, Z. X. Hao, and W. Gong, 2008: Characteristics of anomalous precipitation events over eastern China during the past five centuries. *Climate Dyn.*, **31**(4), 463–476.

Shindell, D. T., G. A. Schmidt, M. E. Mann, and G. Faluvegi, 2004: Dynamic winter climate response to large tropical volcanic eruptions since 1600. *J. Geophys. Res.*, **109**, D05104, doi: 10.1029/2003JD004151.

Sun, Y. and T. J. Zhou, 2014: How does El Niño affect the interannual variability of the boreal summer Hadley Circulation? *J. Climate*, **27**, 2622–2642.

Uccellini, L. M., and D. R. Johnson, 1979: The coupling of upper and lower tropospheric jet streaks and implication for the development of severe convective storms. *Mon. Wea. Rev.*, **107**, 682–703.

Wallace, J. M., and P. V. Hobbs, 1977: *Atmospheric Science: An Introductory Survey*. Academic Press, 483 pp.

Wang, H. J., 2000: The interannual variability of East Asian monsoon and its relationship with SST in a coupled atmosphere–ocean–land climate model. *Adv. Atmos. Sci.*, **17**(1), 31–47.

Wang, H. J., 2001: The weakening of the Asian monsoon circulation after the end of 1970's. *Adv. Atmos. Sci.*, **18**(3), 376–386.

Wang, H. J., and K. Fan, 2013: Recent changes in the East Asian monsoon. *Chinese J. Atmos. Sci.*, **37**(2), 313–318. (in Chinese)

Wang, T., O. H. Otterå, Y. Q. Gao, and H. J. Wang, 2012: The response of the North Pacific decadal variability to strong tropical volcanic eruptions. *Climate Dyn.*, **39**(12), 2917–2936.

Wang, T., H. Wang, O. Otterå, Y. Gao, L. Suo, T. Furevik, and L. Yu, 2013: Anthropogenic agent implicated as a prime driver of shift in precipitation in eastern China in the late 1970s. *Atmos. Chem. Phys.*, **13**(5), 11 997–12 032.

Wu, S., Y. Yin, D. Zheng, and Q. Yang, 2006: Moisture conditions and climate trends in China during the period 1971–2000. *Int. J. Climatol.*, **26**(2), 193–206.

Xu, Q., 1986: The abnormal weather of China for summer 1980 and its relationship with the volcanic eruptions of Mount St. Helens. *Acta Meteorologica Sinica*, **44**, 426–432. (in Chinese)

Xu, Q., 2001: Abrupt change of the mid-summer climate in central east China by the influence of atmospheric pollution. *Atmos. Environ.*, **35**(30), 5029–5040.

Xue, F., 2001: Interannual to interdecadal variation of East Asian summer monsoon and its association with the global atmospheric circulation and sea surface temperature. *Adv. Atmos. Sci.*, **18**(4), 567–575.

Yang, L. M., and Q. Y. Zhang, 2007: Anomalous perturbation kinetic energy of Rossby wave along East Asian westerly jet and its association with summer rainfall in China. *Chinese J. Atmos. Sci.*, **31**(4), 586–595. (in Chinese)

Yoshimori, M., T. F. Stocker, C. C. Raible, and M. Renold, 2005: Externally forced and internal variability in ensemble climate simulations of the Maunder Minimum. *J. Climate*, **18**(20), 4253–4270.

Yu, L., Y. Q. Gao, H. J. Wang, D. Guo, and S. L. Li, 2009: The responses of East Asian Summer monsoon to the North Atlantic meridional overturning circulation in an enhanced freshwater input simulation. *Chinese Science Bulletin*, **54**(24), 4724–4732.

Yu, R. C., B. Wang, and T. J. Zhou, 2004: Tropospheric cooling and summer monsoon weakening trend over East Asia. *Geophys. Res. Lett.*, **31**(22), L22212, doi: 10.1029/2004GL021270.

Zhang, D., R. Blender, and K. Fraedrich, 2013: Volcanoes and ENSO in millennium simulations: Global impacts and regional reconstructions in East Asia. *Theor. Appl. Climatol.*, **111**, 437–454.

Zhang, F. G., and X. G. Zhang, 1994: The relation between large volcanic eruption in the world and the drought/flood in summer in China. *J. Nat. Disasters*, **3**, 40–46. (in Chinese)

Zhang, X. G., and F. G. Zhang, 1985: The relationship between large volcanic eruptions and the dryness/wetness and cold/warm in China. *Acta Meteorologica Sinica*, **43**(2), 196–207. (in Chinese)

Zhang, Y., T. Li, and B. Wang, 2004: Decadal change of the spring snow depth over the Tibetan Plateau: The associated circulation and influence on the east Asian summer monsoon. *J. Climate*, **17**(14), 2780–2793.

Zhang, Y. C., X. Y. Kuang, W. D. Guo, and T. J. Zhou, 2006: Seasonal evolution of the upper-tropospheric westerly jet core over East Asia. *Geophys. Res. Lett.*, **33**, L11708, doi: 10.1029/2006GL026377.

Zhang, Y. C., and D. Q. Huang, 2011: Has the East Asian westerly jet experienced a poleward displacement in recent decades? *Adv. Atmos. Sci.*, **28**(6), 1259–1265.

Zhou, T., and Z. Li, 2002: Simulation of the East Asian summer monsoon using a variable resolution atmospheric GCM. *Climate Dyn.*, **19**(2), 167–180.